Accepted Manuscript

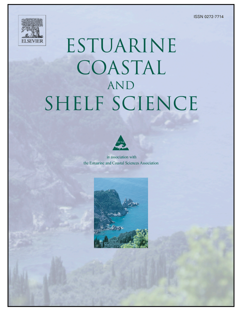

Variations in wave climate as a driver of decadal scale shoreline change at the Inskip Peninsula, southeast Queensland, Australia

Sarah McSweeney, James Shulmeister

PII: S0272-7714(17)31148-4

DOI: 10.1016/j.ecss.2018.04.034

Reference: YECSS 5838

To appear in: *Estuarine, Coastal and Shelf Science*

Received Date: 8 December 2017

Revised Date: 30 March 2018

Accepted Date: 27 April 2018

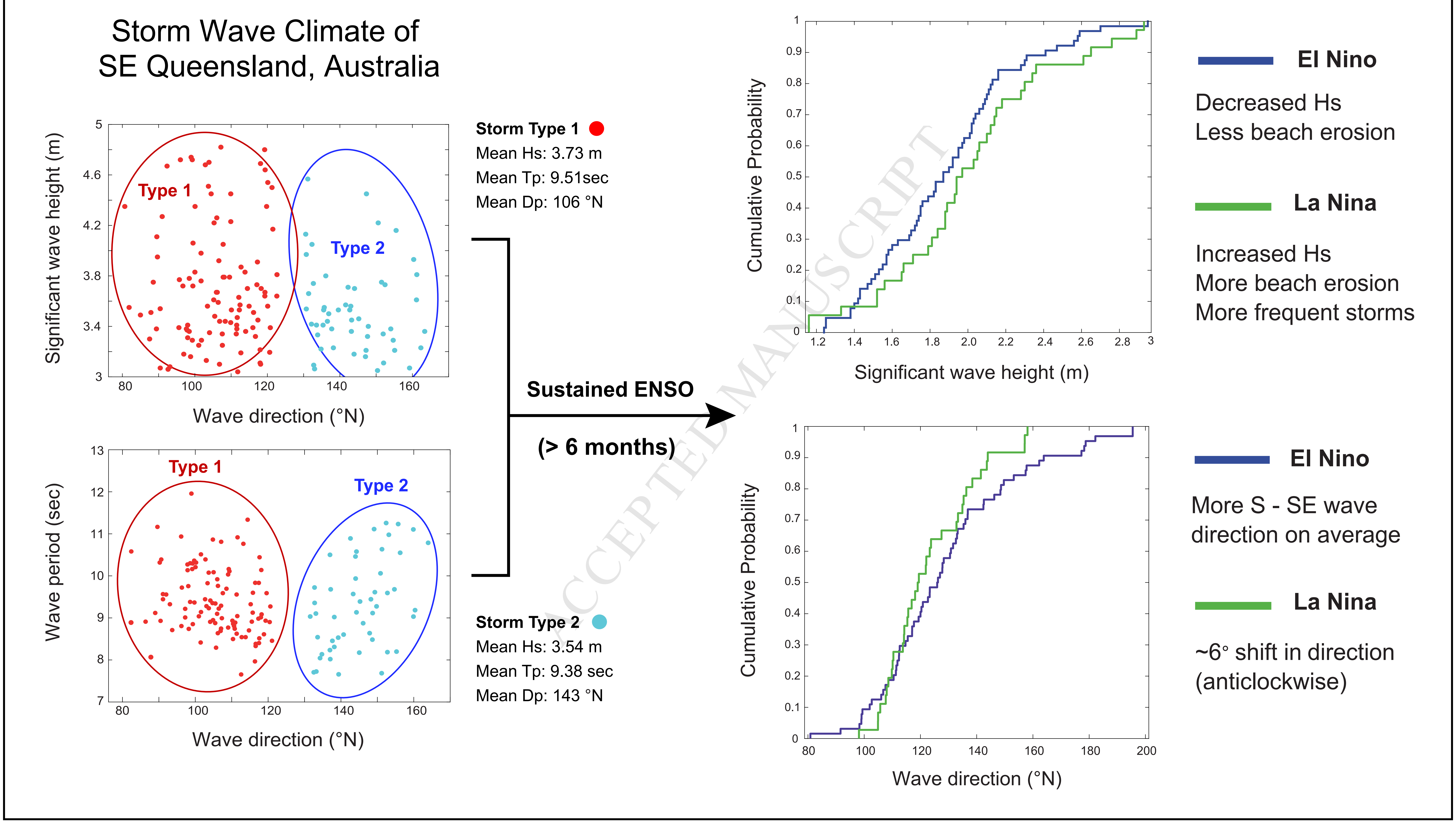
Storm Wave Climate of
SE Queensland, Australia
Significant wave height (m)
Wave direction (°N)
Type 1
Type 2
Wave period (sec)
Wave direction (°N)
Type 1
Type 2
Storm Type 1
Mean Hs: 3.73 m
Mean Tp: 9.51sec
Mean Dp: 106 °N
Storm Type 2
Mean Hs: 3.54 m
Mean Tp: 9.38 sec
Mean Dp: 143 °N
Sustained ENSO
(> 6 months)
Cumulative Probability
Significant wave height (m)
El Nino
Decreased Hs
Less beach erosion
La Nina
Increased Hs
More beach erosion
More frequent storms
Cumulative Probability
Wave direction (°N)
El Nino
More S - SE wave
direction on average
La Nina
~6° shift in direction
(anticlockwise)

Variations in wave climate as a driver of decadal scale shoreline change at the Inskip Peninsula, southeast Queensland, Australia.

Sarah McSweeney[ab] and James Shulmeister[b]

[a]School of Geography, The University of Melbourne, 221 Bouverie Street, Parkville 3010, Victoria, Australia

[b]School of Earth and Environmental Sciences, The University of Queensland, St. Lucia 4072, Queensland, Australia

Corresponding author: Sarah McSweeney

Email: sarah.mcsweeney@unimelb.edu.au

Phone: +61 3 9035 9781

Present address: School of Geography, The University of Melbourne, 221 Bouverie Street, Parkville 3010, Victoria, Australia

1.0 Introduction

Waves provide an important process of energy transfer at the ocean-land interface. The transfer of energy from deep-water to the nearshore is controlled by the offshore wave height, direction, and period, as well as the underlying coastal bathymetry. Wave energy is a key driver of morphological change along global coastlines and understanding the temporal and spatial variability within a wave climate is essential for informed coastal management (Gurran, 2008; Harvey and Woodroffe, 2008; Hugo, 2008; Hemer et al., 2013). While sea level fluctuations have received widespread global attention as a driver of shoreline change, variability in wave climate is expected to be the main process influencing coastal morphodynamics on moderate to high-energy sandy coasts globally (Coelho et al., 2009; Hemer et al., 2012; Mortlock and Goodwin, 2015). Changes in both the height and direction of future storm wave climates have potential to act as drivers in large-scale coastal reorganisation.

A regional wave climate consists of both modal conditions, and conditions specifically related to storm events. While storms provide the energy to mobilise sediment and initiate rapid coastal change, the modal conditions are responsible for beach recovery and the redistribution of sediment onshore (Ranasinghe et al., 2004; Short and Trembanis, 2004). Additionally, a regional storm wave climate may be comprised of several sub-climates originating from a range of directions and synoptic weather systems (Goodwin, 2005; Mortlock and Goodwin, 2015). Differentiating between the sub-types of storm wave climates provides a mechanism of classifying storms as based on their relative frequency and intensity, and ultimately their potential to modify the coast. Although higher energy storms generally tend to induce more substantial beach erosion, other parameters have the capacity to influence the morphodynamic response of the receiving coastline including the storm duration, timing between storm events, wave direction, wave period, and coastal orientation (Short et al., 2000; Cooper et al., 2004). For example, higher incident wave power can increase shoreline erosion rates (Sanford and Gao, 2017) and deep-water waves of a moderate intensity but an anomalous direction can drive substantial beach erosion (Harley et al., 2017). The local planform of a coast can also determine the response to storm impacts (Goodwin et al., 2006; Thomas et al., 2010. For example, headlands can refract waves to alter the nearshore wave direction, as well as change the total energy reaching the nearshore and the proportion of cross vs alongshore transport, and therefore the capacity of storms from different directions to drive change (Harley et al., 2011; Thomas et al., 2011; Nichol et al., 2016; Davidson et al., 2017). Storm impacts will therefore be determined by the characteristic wave climate of each storm type (i.e. height, direction, duration), and the morphology of each individual coastline.

In this study, the role of variability in the seasonal and decadal wave climate is examined as a driver of shoreline change on the open Fraser coast of southeast Queensland, Australia. The study region provides a proxy for open sandy, drift-dominated coastlines globally with similar counterparts described in New Zealand (Kasper□Zubillaga et al., 2007; Bryan et al., 2008; Tribe and Kennedy, 20101), Brazil (e.g. Santa Catarina coast: Siegle and Asp, 2007), and the U.S.A (Allen, 1981). While a growing body of literature has focused on classifying the wave climate of southeast Australia, most work has focused on New South Wales (NSW) (Harley et al., 2010; Shand et al., 2011; You, 2011; Mortlock and Goodwin, 2015; Pender et al., 2015) and the Gold Coast (Allen and Callaghan, 1999; Straus et al., 2007; Splinter et al., 2012). In southeast Australia, three distinct modal wave climates are recognised: (1) E-ESE (direction of 85-105°N, short wave periods of 8-9 secs); (2) ESE-SSE (direction of 110-150°N, long periods of 11-12 secs); and (3) SE-SSE (direction of 140-160°N, moderate periods of 9-10 secs) (Shand et al., 2011; Mortlock and Goodwin, 2015; Pender et al., 2015). Storms waves are generated by: (1) easterly trough lows, also known as 'east coast lows'; (2) extratropical cyclones; (3) southern secondary lows; (4) inland troughs; and (5) continental lows, with storm types 3-5 increasing in dominance further south along the Australian coast (Splinter et al., 2012; Browning and Goodwin, 2013). Due to a lack of long-term directional wave data, our understanding and classification of these wave climates is often applied to other sectors of the southeast Queensland coast. A shortcoming of this is that for regions located north of Brisbane (-27.45°S, 153.03°E), latitudinal differences result in a shift in regional synoptic conditions that are not accounted for. For example, the Queensland coast north of Brisbane fundamentally differs from NSW as it is more exposed to wave trains propagating from tropical cyclones generated in the Coral Sea (Mortlock and

Goodwin, 2015) with the potential to cause major episodes of coastal erosion (Splinter et al., 2012; Nott et al., 2013).

A further underlying control on the variability in wave climate and storm frequency is the El Nino Southern Oscillation (ENSO). In southeast Queensland, it has been suggested that during El Nino events, increased jetstream activity may help trigger more east coast lows, reduce the number of tropical cyclones, and alter the mean wave direction (Allen and Callaghan, 1999; Short et al., 2000; You and Lord, 2008). In northern NSW, El Nino years (Southern Oscillation Index (SOI) ≤ -7) have been linked to periods of lower wave height and an increase in the southerly wave component (i.e. a clockwise rotation in wave direction), while La Nina (SOI ≥ 7) tends to result in higher waves with a dominant easterly direction (i.e. an anticlockwise shift in wave direction) (Ranasinghe et al., 2004). The change in wave height and direction resulting from ENSO variability in southeast Australia has been linked to decadal scale beach rotation with alternating accretion (erosion) occurring at opposite ends of beaches (Ranasinghe et al., 2004; Short and Trembanis, 2004). ENSO impacts on wave climate variability have not yet been investigated north of Brisbane where its impact on storm frequency and wave height, particularly as associated with ex-tropical storms, could be expected to be equally if not more strongly, correlated. In terms of translating the effects of wave climate variability to the morphological response of the shoreline, most prior work in Australia has been undertaken where sediment transport occurs largely within an embayed cell (Short et al., 2000; Short and Trembanis, 2004; Daly et al., 2015; brd et al., 2015) as well as internationally (Ojeda and Guillén, 2008; Loureiro et al., 2009; Pinto et al., 2009). As many beaches in southeast Queensland are located along open coastlines (e.g. Noosa, Sunshine Coast, and the majority of beaches on Fraser and Stradbroke Islands), it is logical that shoreline response to wave climate variability be determined from an open coast analogue. The Interdecadal Pacific Oscillation (IPO) is a further long-term (15-30 and 50-70 years) climatic oscillation which interacts with ENSO related climate variability (Grant and Walsh, 2001; Salinger et al., 2001; Power et al., 2006). Specifically, negative phases of the IPO increase sea-surface temperatures off Queensland and enhance La Nina events, whereas positive phases are associated with cooler water and reduced extra-tropical storm activity.

The present study aims to: (1) identify the wave climate for southeast Queensland based on a 31 year hindcast wave dataset; (2) delineate between different storm climates; (3) consider the role of ENSO as a driver of variation in wave climate; and (4) identify rates and trends of decadal scale shoreline change in response to temporal variability in wave conditions. The identification of different storm wave climates will enable a better understanding of events which most strongly impact upon the shoreline and will provide a baseline for future comparison. For instance, small changes in the directional wave height will have implications for the coastal sediment budget and consequentially beach morphodynamics. An important consideration is the change that may occur under projected shifts in global climate, such as an increase in the extra-tropical migration of tropical cyclones and in the frequency of storm events (Hughes, 2003; Harvey and Woodroffe, 2008; IPCC, 2013).

1.1 Regional setting

The open coast of southeast Queensland, Australia, is wave-dominated and microtidal with a spring tidal range of 1.35-1.86 m (Harris et al., 2002). The coastal climate is classified as humid subtropical, consisting of warm, humid summers and mild winters (Peel et al., 2007). The present-day storm wave climate is influenced by the occurrence of tropical cyclones during November-April, most of which develop in the Coral Sea and track southward. On average, about three cyclones per year are observed in the Coral Sea with wave fields impacting the southeast Queensland coast (Allan and Callaghan, 1999), although the number of cyclones which actually make landfall is typically <1 per year (Flay and Nott, 2007). East coast lows are a further storm type influencing the coastline and result from trough intensification over eastern Australia. The interaction of east coast lows with developing high pressure systems to the south can increase the severity and duration of coastal storms (Short and Trenaman, 1992; Callaghan and Power, 2014).

While the wave data in this study are representative of southeast Queensland as a whole, a specific compartment of the coast was used to map decadal scale shoreline change in close proximity to where the wave data was extracted from (Figure 1). The shoreline study area consists of a 15 km stretch of sandy beach along the Inskip Peninsula (Figure 1). The study coastline is unmodified and representative of the open drift-aligned southeast Queensland coast. It is bounded by the Great Sandy Strait to the north, a significant tidal channel which separates mainland Queensland from Fraser Island, and the Double Island Point headland to the south. Tides are semidiurnal with a mean spring tidal range of 1.40 m (at Rainbow Beach) and a HAT of 2.28 m (Queensland Government, 2017a). The east Australian longshore drift system carries approximately 500,000 m^3 of sand per year from the Gold Coast north towards Fraser Island where the subaqueous Breaksea Spit represents the northern terminus (Boyd et al., 2008). The net longshore drift direction is to the north with sediment being supplied from NSW coastal catchments (Roy and Crawford, 1977; Roy and Thom, 1981). Ebb-tidal flows through the Great Sandy Strait also rework and transport sediment seaward from the adjacent Hervey Bay where it is then moved offshore and northward to Fraser Island (Boyd et al., 2008). The East Australian Current flows south from the Coral Sea along the edge of the continental shelf, until it reaches central NSW (Cresswell et al., 1983; Church, 1987). The East Australian Current is located 10 km offshore near Fraser Island to the north and approximately 20-30 km offshore of the Inskip Peninsular (Boyd et al., 2008).

2.0 Material and methods

2.1 Wave data

A 31 year (1979-2009) hindcast wave record was obtained from the third-generation wave model NOAA WAVEWATCH III (WWIII) (CFSR Reanalysis Hindcasts) (Tolman, 2009; Chawla et al., 2012). WWIII is widely accepted as a reliable source of hindcast data across a variety of settings (Browne et al., 2007; Strauss et al., 2007; Cornett, 2008; Sofian and Wijanarto, 2010; Arinaga and Cheung, 2012) and in Australia, shows good agreement with satellite altimetry, visual observations and wave-rider buoy data (Hemer and Church, 2007; Hughes and Heap, 2010). WWIII uses high resolution (1/2°) global winds at 10 m height from the NCEP Climate Forecast System Reanalysis (CFSR) along with a coupled reanalysis of the atmospheric, oceanic, sea-ice, and land data (Chawla et al., 2012). Hindcast data from WWIII includes a bias-correction based on collocated altimeter data which reduces error for high-wind speeds (Chawla et al., 2012). Hindcast wave data was taken from -25.90 °S, 153.73 °E (in >25 m water depth) using the Australia four arc minute grid at a resolution of 1/15° x 1/15° (Figure 1). The grid point was selected to be as close as possible to the study shoreline while allowing waves to maintain the most direct and uninhibited passage onshore. Data was extracted from grib format and analysed in MatLab R2015b software to output the mean daily significant wave height (Hs), primary peak spectral wave period (Tp), and average direction at the peak period (Dp) which was then presented as an overall time series. From this dataset overall mean daily and mean monthly descriptive statistics wave were calculated.

2.2 Delineation of storm and modal conditions

Within the wave dataset, individual storm events were extracted for further analysis. Storm events were separated from modal wave conditions using a modified Peaks-Over-Threshold (POT) method (after Mortlock and Goodwin, 2015). POT analysis aims to identify storm events in a continuous wave record that exceed a certain Hs threshold, are maintained for a minimum duration, and that are separated by a minimum recurrence interval.

The critical Hs storm threshold was selected at 2.93 m. This value represents the daily 10 % exceedance wave height (Hs_{10}) as calculated from Hs exceedance probability analysis of the 31-year dataset. Hs_{10} has been recommended as an appropriate threshold to categorise storms for southeast Australia by Mortlock and Goodwin (2015). Other critical storm thresholds considered were 3 m and the 95th percentile wave heights. The 3 m and 95th percentile scenarios, however, proved to greatly reduce the number of individual storm events. The Generalised Pareto Distribution (GDP) was used to further verify the statistical robustness of the selected threshold level based on the goodness-of-fit as per Coles et al. (2001) and Mazas and Hamm (2011). To classify storm events within the wave data record, a minimum storm duration of 3 days was chosen based on other southeast Australian wave climate and synoptic analyses (Hemer, 2010; Shand et al., 2011, Mortlock and Goodwin, 2015) and a minimum recurrence interval of 24 hours.

2.3 Classification of storm wave climates

After identifying each individual storm event within the time series (as per Table 1), the mean Hs, Tp, and Dp were normalised following the methods of Camus et al. (2011). Data normalisation was undertaken to ensure equal weighting was given to each parameter by providing a range for all parameters between 0 - 1. Prior to clustering, the optimal number of clusters was first identified using a Silhouette analysis (Rousseeuw, 1987) and gap statistics (Tibshirani et al. 2001) run on MatLab R2015b software. The Calinski-Harabasz criterion clustering evaluation was run in MatLab R2015b for 2 - 8 clusters. All methods indicated that two clusters was the optimum grouping for the dataset. Using the normalised Hs, Tp, and Dp values , storm events were classified into groups using a K-means clustering method undertaken using IBM SPSS Statistics 23 software. K-means was selected based on its use in prior wave classification studies which also consider storm origin and synoptic typology (e.g. Goodwin and Mortlock, 2015). The K-means cluster was run using the identified optimum number of groupings to output cluster centres for each group and to identify how many storm events were classified within each group.

As K-means clustering indicated that the wave direction was the strongest driver of cluster delineation. The distribution of wave directions occurring for the whole storm dataset were plotted as a probability density function (PDF) and this too showed a bimodal distribution (both as normalised data and as ° from N for each storm event). Circular statistics were run through CircStat (Berens, 2009) to confirm that the storm wave climate groupings were statistically different. Gaussian Mixture Models (GMM) were also run in MatLab R2015b to determine cluster centres for the parameters Hs, Tp, and Dp. The GMM produced similar cluster centres to K-means. Descriptive statistics of Hs, Tp, and Dp for each grouping were then calculated and converted to de-normalised data form. The mean duration and seasonality of storm occurrence was then extracted from the storm record using the groupings output from GMM, CircStat, and K-means. Non-metric multidimensional scaling (nMDS) and hierarchal cluster analysis were also performed (Clarke and Warwick, 1994) as a final comparison to the groups classified using K-means and GMM (see supplementary material).

2.4 SOI comparison

A 56-year record (1957-2012) of the mean monthly SOI was downloaded from Bureau of Meteorology (BoM) (2017) for comparison to wave parameters. The mean annual SOI was compared to the mean annual Hs, Dp, Tp, days with a mean daily Hs >Hs_{10} (days >Hs_{10}), and storm frequency and duration using a Pearson correlation analysis. Mean annual data were used to account for intra annual variability and to correspond with the annual scale interval of aerial imagery. To determine the specific impacts of El Nino and La Nina events on variability in the wave climate, the mean monthly SOI index for periods of El Nino (SOI index $\leq$ -7) and La Nina (SOI $\geq$ 7) were extracted from 1979-2009. A six-month minimum threshold was applied. This was used as it has been shown that in southeast Australia, El Nino and La Nina events must be sustained for several months to be reflected in the wave climate with a phase lag occurring before these impacts become apparent (Ranasinghe et al., 2004). The shifts in wave height and direction during the periods of sustained El Nino and La Nina were plotted as PDFs with descriptive statistics calculated.

To analyse the lag time for changes between the SOI and mean monthly sea surface temperature (SST), a cross correlation analysis was performed in MatLab R2015b. Mean monthly SOI values from BoM were compared to the mean monthly SST (1957-2012) obtained from the NOAA Extended Reconstructed SST (ERSST) v.4 dataset. SST data were extracted from -26 °S, 153.73 °E, the closest available location to the WWIII wave hindcast grid point (±0.01 °S). The lag time for changes in Hs relative to SST (1979-2012) were analysed using the normalised mean monthly Hs. The maximum lag duration was set at +20 and -20 months to incorporate the known window of time (3-17 months) where changes in SOI are reflected in beach morphological response in southeast Australia (Ranasinghe et al., 2004).

2.5 Analysis of decadal scale shoreline change

A 54-year dataset (1958-2012) of aerial imagery from Qspatial (Queensland Government, 2017b) was used to analyse decadal shoreline change for the 15 km long Inskip Peninsula beach (Figure 1). Images were available for 20 individual years between 1958-2012. The average duration between images was three years but there a longer duration (>5 years) existed for images taken 1996-2012. Aerial images were georectified in Arc GIS v.10.3.1 using a bilinear interpolation method. Each image was georectified with at least six control points and a maximum RMS error of 3.90 m. Shorelines were digitised in ARC GIS and then analysed using the Digital Shoreline Analysis System (DSAS) Version 4.0 (Thieler et al., 2009). The high water mark (HWM) was used to represent the shoreline position (after Moore et al., 2006). The HWM is widely regarded as the most reliable indicator of shoreline position due to its ability to be easily detected using aerial imagery (Crowell et al., 1991; Pajak and Leatherman, 2002; Fletcher et al., 2003). As the HWM can be influenced by sea level elevation, all dates of aerial imagery were checked against historic sea level records using the Mooloolaba and Noosa Heads gauges. The HAT was not exceeded at any time of the aerial imagery dates.

Using DSAS, the oldest shoreline position (1958) was buffered 400 m landward to create a baseline. 150 transects were cast along the beach at 100 m intervals to cover the shoreline extent. Each shoreline was weighted by the RMS error of the georectified imagery. The least median of squares method was calculated using DSAS to find the rate of shoreline change for the whole beach. The least median of squares method uses the median value of the squared residuals instead of the mean to determine the best-fit equation. This method was selected over linear regression as it more tolerant to outliers and large variations in beach width (Thieler et al., 2009). The net change in shoreline movement was then compared to temporal variability in the SOI, wave direction, and significant wave height.

3.0 Results

3.1 Overall wave climate

From the hindcast wave dataset, the dominant wave direction at the study location is from the SE (mean Dp = 129 °N) with a mean Hs of 1.91 m and Tp of 8.60 sec (Table 1). Throughout the year, the wave direction varies from being predominantly ESE during January to March, to shift to the SE in

April to December (Figure 2a). Peak wave heights occur during January to July, with Hs in February to May exceeding 2 m on average (2.09-2.25 m) (Figure 2b). The lowest waves coincide with a more south-easterly direction during September to October (Dp = 145 °N; Hs = 1.57-1.61 m) (Figure 2a-b). Longer period waves occur during January to August (T = >8.45 secs) with a shorter period more prevalent in September to December (T = <8.40 secs) (Table 1; Figure 2c).

3.2 Storm wave climate classification

157 individual storm events were observed during 1979-2009 at an average frequency of 5.1 storms per/year and duration of 4.4 days. Storm wave directions show a bimodal distribution with a dominant E-ESE peak and a second peak from the SE (Figure 3a). In terms of the directional wave height, storms associated with an E-ESE direction tended to show the largest wave heights (Figure 3b).

Using a K-means cluster analysis on normalised data, two distinct clusters occurred after three iterations (Figure 4). The wave direction was the primary driver of this delineation (Figure 4). Circular statistics indicated that the mean wave direction for the two wave climates were statistically different (p = <0.01) and produced mean values for each group that were ±1° similar to those identified using K-means (Table 2). GMM showed very similar cluster centres to K-means for all parameters with 1° difference in Dp, <0.05 m difference in Hs, and <0.03 sec difference in Tp (Table 2; Figure 5a-b). The GMM also confirmed that the two groupings also correspond with statistically significant wave heights and periods (Figure 5a-b; Table 2). The two groupings of storm wave climates are referred to as Type 1 (E-ESE climate) and Type 2 (SSE-SE).

3.3 SOI impacts on wave climate variability

The mean annual SOI index shows a strong positive correlation with wave height (r = 0.505, p = <0.01) as well as the number of days exceeding the Hs_{10} threshold (2.93 m) (r = 0.422, p = <0.05) indicating that positive SOI years have higher waves on average (Table 3). Mean annual SOI showed a negative correlation with wave direction (r = -0.362, p = <0.05) indicating that years with positive SOI tend to experience waves propagating from a more easterly direction on average (Table 3). The annual storm frequency was also positively correlated with the SOI index ($r = 0.367$, $p = <0.05$) (Table 3).

Periods of sustained (≥6 months) El Nino results in lower wave heights on average (mean Hs 1.88 m, median 1.87 m) while La Nina events tend to coincide with periods of higher waves (mean Hs 2.01 m, median 1.97 m) (Figure 6a). In terms of wave direction, periods of sustained El Nino sees an increase waves from the S-SE on average (mean Dp 130 °N, median 128°N), while La Nina tends to result in a shift in wave direction favour a more easterly direction (mean Dp 123 °N, median 119°N) (Figure 6b).

3.4 Shoreline change

The overall rate of shoreline change during 1958-2012 for the Inskip Peninsula shows a mean erosion rate of 0.29 m/year (Figure 7a). The distribution of the rates of shoreline change across the study area is both spatially and temporally variable, with both the north and south ends of the beach showing the highest rates of erosion (Figure 7b-c).

On average, periods of larger waves from a more easterly direction coincide with higher net erosion at the Inskip Peninsula (Figure 8b-c). While the SOI did not directly correlate with shoreline change, in the 6 months-1 year following periods of El Nino, the beach tends to accrete (Figure 8a). In the 5-6 months' time following a La Nina event, accelerated erosion is visible (Figure 8a). Temporally, the beach showed most accretion during 1990 to 1991 with a net change in shoreline position of +19 m (± 3 m). Between 1 Aug 1990-11 Sep 1991, the SOI remained negative to neutral (mean SOI of -1.32 throughout this period), the SST anomaly was -0.03°C on average, and lower waves occurred on average with a mean Hs of 1.82 m (compared to the overall mean of 1.91 m).

The most severe shoreline retreat occurred from 11 Sep 1991-26 May 1994 with a net change of -17 m (±2.84 m). Beach erosion at this time is likely due to the clustering of three storms that occurred in rapid succession in the 6 months prior to the 1994 imagery (8-10 Dec 1993, 25-29 Jan 1994, and 21-31 Mar 1994). The duration of the final storm preceding the 1994 aerial image (21-31 Mar 1994) was

11 days which was the longest duration storm that occurred within the record. The SST anomaly for the winter of 1993 was > +0.75°C (Figure 8a). This provided a period of sustained high SST that may have facilitated the 1993/1994 summer storm events. To support this, the mean annual SST anomaly shows a positive correlation with the annual storm frequency ($r = 0.450$, $p = >0.05$) (Table 3). Although the net change in shoreline movement was high between 1991-1994 images, the shoreline position in 1994 relative to the 1958 baseline was +0.42 m.

3.5 Cross correlation of SOI, SST anomaly, and Hs

A mean monthly SST anomaly of > +1°C tended to precede La Nina events, periods of higher Hs, and a retreat in net shoreline position (Figure 8a-c). Cross correlations between the mean monthly SOI and the mean monthly SST anomaly indicate that the two parameters are best correlated ($r = -0.29$) when change in the SOI leads SST by 9 months (Figure 8d). When the SOI lags changes in the SST, the maximum correlation ($r = 0.27$) occurs at 4 months. The mean monthly SST anomaly shows a maximum cross correlation with the mean monthly Hs anomaly ($r = 0.24$) at a 6-month lag period (Figure 8f). This indicates that it takes approximately 6 months for changes in the SST to influence a higher Hs at the study location. To test the 6-month lag impacts on shoreline movement, the net shoreline movement was correlated with monthly means of the SST and Hs anomalies, Hs, Dp, Tp, and SOI using the average value for the 6 months preceding the image date (Table 3). The SST and Hs anomalies were positively correlated ($r = 0.616$, $p = <0.05$) and both the SST ($r = -0.592$, $p = <0.05$) and Hs ($r = -0.646$, $p = <0.05$) anomalies were negatively correlated with the net shoreline movement (Table 3). This indicates that shoreline retreat at the study location typically occurs following higher than average SSTs and Hs in the 6 months prior.

4.0 Discussion

4.1 Storm wave climates

Type 1 synoptically translates into storm wave fields associated with ex-tropical storm activity in the Coral Sea. Type 1 storms are most prevalent during late summer-early autumn with Hs being >3.7 m.

The direction of Type 1 storms favours an E-ESE approach with most waves (85 %) occurring from 98-110 °N (Table 2). Although many ex-tropical storms in the region tend to track south from the equator, an absence of a strong N-NE signal in storm wave direction may be attributed to the blocking influence of Fraser Island to the north. Based on the hindcast wave dataset, the average return interval (ARI) for a Type 1 storm with an average Hs >3.8 is 2 years and for Hs >4 m, the ARI is 4 years (see supplementary material). These values are comparable to those of Allen and Callaghan (1999) who estimate an ARI of 2 years for tropical storms with Hs >3.9 m and 5 years for Hs >4.6 m in southeast Queensland. Type 1 storms have a mean wave period of ~9.4 secs with similar wave periods of 9-10 secs being described for E-SE waves on the southeast Queensland coast (at Brisbane) (Mortlock and Goodwin, 2015). Compared to northern NSW, the wave period is longer in southeast Queensland for E-ESE waves as attributed to uninhibited swell wave propagation from the Equatorial Pacific and Coral Sea (Speer et al., 2009).

Type 2 represents coastal lows of a SSE-SE direction and correspond with east coast lows (Shand et al., 2011; Browning and Goodwin, 2013). The majority of Type 2 storms (70 %) propagate from 138-148 °N with Hs being <3.8 m for 88 % of all Type 2 storms (Table 2). This corresponds with the findings of Gourlay (1975) where waves from the E observed at Moffat Beach (100 km S of Inskip Peninsula) displayed higher Hs than waves from the SE. Based on the hindcast wave dataset, the ARI for a Type 2 storm with an average Hs >3.5 m is 3.8 years (see supplementary material).

The storm climates identified in the study region provide an important analogue for understanding storm wave variability in other regions of southeast Queensland. The study provides the first analysis of the long-term wave climate and subtropical storm wave record north of Brisbane. The two classified storm climates correspond with those identified by Splinter et al. (2012) for the Gold Coast region. A fundamental difference between the Inskip wave climate and that of the Gold Coast is that a higher proportion of storms are associated with ex-tropical storm activity as opposed to east coast lows which are dominant at the Gold Coast and further south in NSW. This is a predictable outcome. When applying the POT threshold to identify storms, waves propagating from a purely southerly direction did not reach the threshold for being classified as storm events. This is because the Inskip Peninsula lies above the swell window for storm waves associated with Southern Ocean Lows (Browning and Goodwin, 2013). Seasonally, the highest proportion of storms occur during January-May (see supplementary material) irrespective of storm type. While southerly waves are at times present during modal conditions, it is likely that by the time storms of a southerly origin have propagated to reach the study region their energy has dissipated - potentially due to refraction across the continental shelf from NSW northward. Evidence of this is that Type 2 storms, which have a SE-SSE direction on average, have a shorter period (T = <9.4 sec) and lower height (and therefore would have a lower wave energy and power) than SE-S storms occurring in NSW (T = 11-12 sec) (Morlock and Goodwin, 2015). Local morphology may also play a role in this as waves of a more southerly origin may be refracted around Double Island Point therefore reducing their wave height and energy upon reaching the coastline.

4.2 Impact of ENSO on wave climate

ENSO variability is known to influence wave height and direction in southeast Australia with negative phases linked to an anticlockwise shift in wave direction and a decrease in wave height (Phinn and Hastings, 1992; Short et al., 2000; Ranasinghe et al., 2004; Goodwin 2005; You and Lord, 2008; Harley et al., 2010). While this relationship has been the focus of a growing body of literature, the role of ENSO in driving wave climate variability has not been well defined in subtropical regions north of Brisbane (27.47 °S). In the present study, ENSO showed a strong positive correlation with mean annual wave height and a negative correlation with wave direction (Table 3). The correlation between mean annual Hs and SOI was the strongest of all ($r = 0.505$, $p = <0.01$) (Table 3) and is also higher than that the same correlation undertaken for a 45-year wave record at Sydney, NSW, by Harley et al., (2010) ($r = 0.39\text{-}0.43$, $p = <0.01$). This indicates that ENSO has a stronger influence on wave heights at lower latitudes where the SST is warmer. During periods of sustained La Nina events, the shift in distribution of wave height and direction was more substantial than during El Nino events with a 0.1 m increase in mean Hs and a 6° anticlockwise shift in mean wave direction occurring (relative to the overall mean (Table 3).

The coupled shift to an easterly direction with higher wave heights during positive SOI phases also reflects a higher occurrence of ex-tropical storms (Table 3). Interestingly, mean annual storm duration showed a moderate negative correlation with SOI ($r = -0.357$, $p = <0.05$) (Table 3). This is the opposite of what would be expected as Type 1 storms have a longer duration on average and are representative of storm wave conditions positively correlated to the SOI (i.e. E-ESE, higher Hs) (Table 2; Table 3). This indicates that annual scale SOI data is not a good predictor of storm duration and that additional local synoptic factors are likely to influence the longevity of individual storm events. For example, the interaction of storms with adjacent areas of high pressure, including the subtropical ridge, is known to influence storm severity and duration (Allen and Callaghan, 1999; Walsh et al., 2004).

These findings have highlight the importance of understanding large scale climate processes on other subtropical coastal regions globally affected by wave trains associated from extra-tropical storms. This extends to the Northern Hemisphere where the North Atlantic Oscillation (NAO) similarly controls westerly wind (and wave) characteristics and the location of storm tracks across the North Atlantic. During positive (negative) NAO phases the North Atlantic storm track would be expected to shift northwards (southwards) (Lehmann and Coumou, 2015). Extratropically transitioning tropical cyclones represent 50% of all tropical cyclones that make landfall on the east coasts of the U.S.A, Canada, and the west coast of Europe. Variability in the NAO also relates to shoreline change with the potential to drive beach rotation (Thomas et al., 2011). Evidence that storm tracks in the North Atlantic are shifting southward over the last several decades (Clarke et al., 2002; Hurrell et al., 2003; Costas et al., 2006).

4.3 Shoreline change

The shoreline response to decadal scale variability in wave climate provides an important analogue for other wave-dominated beaches along the open southeast Queensland coastline and in particular, for regions north of Brisbane. During 1958-2012, the Inskip Peninsula has shown a trend of beach erosion at a rate -0.29 m/year on average (Figure 7a). Higher net erosion occurred during periods of larger waves occurring from a more easterly direction, while periods of lower wave height resulted in beach accretion regardless of the wave direction (Figure 8a-d). The most substantial erosion also occurred following periods of increased SST anomaly >1°C (Figure 8a). Periods of La Nina (El Nino) did not directly coincide with shoreline retreat (progradation) but tended to lag the peak of La Nina (El Nina) episodes (Figure 8a-b). Interestingly, the centre of the beach shows a trend of net accretion in an area located north of a beach rock formation (Eight Mile Rocks) where there is also a change in coastal alignment (Figure 7a-c: 5-7 km). As the beach rock provides a hard, nodal point, the northward section of the beach could see future coastal compartmentiliation similar to the model of Stephens et al. (1981) for formation of zetaform bays down-drift side of beach rock ourcrops. This would potentially result in the creation of two separate littoral cells while a trend of net erosion persists.

The most severe erosion (-0.73 m/year) occurs at the southern end of at the study beach and in the lee of the Double Island Point headland, a shadow zone from northward moving longshore drift (Figure 7c). The northern end of the beach too shows a long-term trend of net erosion which is unexpected as it would be assumed to be receive more sediment supplied from drift with less refraction from the headland. This illustrates an imbalance in the coastal sediment budget and suggests that we may need to revisit existing sediment budgets for drift dominated shorelines in southeast Queensland. The constant 'river' of sediment that is inferred to be moving north from NSW to Fraser Island does not dominate the signal of coastal accretion and erosion at the study location (Figure 7a-b; Figure 8a). Existing studies suggest that littoral drift rates should increase progressively northwards along the coast of southeast Queensland (Stephens et al., 1981). As the study beach is located near the terminus of the east Australian longshore drift system, we would expect to see normal seasonal cycles of erosion-accretion superimposed upon an either stable or accretionary long-term state. There is however a trend of net erosion punctuated by large (>10 m) interannual changes in shoreline position which are clearly tied to variability in the wave climate (Figure 8a-d). These shifts in shoreline position may be related to sediment slugs moving alongshore. Temporary storage offshore and on beaches and barrier islands such as Moreton, Stradbroke, and Bribie Islands is largely unaccounted for in current models (e.g. Roy and Thom, 1981). A higher demand for longshore sediment supply would likely occur at the Inskip Peninsular if the coast evolved to be further oblique to the dominant swell direction (Stephens et al., 1981) which would intensify coastal erosion. The site provides an important proxy for predicting coastal response to future shifts in wave climate and ENSO events at similar drift-dominated, subtropical coastlines globally, as well as for understanding how beach readjustment can modulate these effects. This is particularly relevant for beaches at the terminus of significant drift systems where sediment supply is determined by down drift processes and coastal alignment (e.g. U.S.A: Stone et al., 1992; Brazil: Martin and Suguio, 1992; west Africa: Blivi and Oyédé, 2002; and South Africa: Smith et al., 2010).

The time elapsed between individual storms proved important in determining the magnitude of shoreline erosion with storms clustered in rapid succession leading to more substantial erosion (e.g. 1994) that individual events of a high magnitude. This is because the recovery period that would facilitate beach accretion was reduced between storm events. This illustrates the importance of the buffering capacity of the beach in preventing substantial erosion both for storms occurring in close succession. This is consistent with observations in southeast Australia (Callaghan et al., 2008; Karunarathna et al., 2014), Europe (Vousdoukas et al., 2012; Dissanayake et al., 2015; Castelle et al., 2015; Masselink et al., 2016), and the U.S.A (Flick, 1993). At the Inskip Peninsula, storm clustering and erosion would extend to the dunes which directly bound the southern portion of the beach however the associated outcomes of their net input to the coastal sediment budget is unknown.

4.4 Future considerations

This study provides a first classification of storm wave climates in the region to correlate storm activity with decadal scale climate drivers and shoreline change. Use of multivariate Neural Network Clustering methods, such as Self Organising Maps (SOM), may offer potential to delineate further between storm types in future (Camis et al., 2011; Liu and Weisberg, 2011). Further delineation between the Type 1 storms identified within this study would be valuable as these events tend to cause the most substantial erosion at the shoreline. Type 1 storms are also most likely to change in frequency and magnitude if there was a southward expansion of the sub-tropics.

Understanding the changes in directional wave height of the two classified storm wave climates has implications for the coastal sediment budget and consequentially beach morphodynamics. A shift in wave height, and most importantly direction, would translate to large changes in the longshore transport flux at the receiving coastline (USACE, 1986; Hemer et al., 2010; Splinter et al., 2012; Splinter et al., 2014). The landward extent of storm waves would also increase under predicted future increases in sea level and storm Hs (due to enhanced wind speeds) (IPCC, 2013) consequentially exacerbating the magnitude of coastal erosion observed in this study. Although detailed nearshore modelling was not undertaken for this work, the study findings provide valuable information that could be used in future to analyse the nearshore conditions for each storm wave climate. For example, a simple application of the CERC (USACE, 1984) equation, shows a +3,235 m^3/day (Type 1) and +431 m^3/day (Type 2) increase in the net longshore drift rate from modal conditions (for details on drift calculations, see supplementary material). This illustrates the potential to result in imbalances to the coastal sediment budget when the northward littoral transport exceeds the amount transported from the south.

5.0 Conclusions

From a 31-year hindcast wave dataset, the present study has established that two storm wave climates are dominant in southeast Queensland: Type 1 (ex-tropical storms) and (2) Type 2 (east coast lows). The storm wave climates show clear differences in mean wave height and direction, with the dominance of Type 1 storms resulting in higher waves and enhanced shoreline erosion. The SOI is an important forcing factor influencing the variability in wave climate, being positively correlated to wave height and storm frequency, and negatively correlated with wave direction. This indicates that Type 1 storms are more prevalent during periods of positive SOI phases with the potential to induce more substantial erosion. During periods of sustained La Nina/El Nino events, shifts in the distribution of wave direction and height become more apparent, with La Nina resulting in higher waves and a more easterly direction, and El Nino corresponding with lower waves from a more southerly-southeast direction. The change in wave height and direction was most pronounced in La Nina phases and corresponds with a +0.10 m increase in mean monthly wave height and a 6° anticlockwise shift in wave direction. These changes are likely to translate into a larger difference in directional wave power at the shoreline with the potential to influence distinct phases of beach erosion, alongshore sediment supply, and coastal sediment budgets. A change in offshore wave direction is known to outweigh a change in wave height when translated to nearshore effects (e.g. nearshore directional spreading or localised refraction) (Wandres et al., 2017).

The observed change in shoreline position through the study period is both spatially and temporally variable. Shoreline deposition (erosion) relates to both short-term storm events and longer-term shifts in the wave climate induced by the underlying signal of the SOI. Following sustained La Nina events, beach erosion occurs on at an average rate of -5.75 m/year (±2.03 m) while following El Nino events, the shoreline is accretionary at an average rate of +4.32 m/year (±2.06 m) (Figure 8b). There is a six-month time lag for changes in the SST, a parameter related to the phase and intensity of the SOI and which causes heightened tropical storm activity (Sohn et al., 2016), to be translated to changes in the Hs. The buffering capacity of the beach and the succession and duration of individual storm events proved to be important in determining the extent of shoreline erosion, with storms occurring in rapid succession favouring more extensive erosion. The study findings have application for similar drift dominated open coastline beaches globally. Future climate warming is predicted to result in widening of the tropics with a poleward expansion of 1-2° projected for later this century (Seidel et al., 2008; Mortlock and Goodwin, 2015). This may lead to an increase in frequency of ex-tropical storm tracks further south and a change in regional wave climates for southeast Queensland and northern NSW. Storm wave parameters from the Inskip Peninsula can therefore provide surrogate data to project future storm wave impacts at more southern locations on the Australian seaboard.

Acknowledgements

ARC Discovery grant. DP150101513. Climate and environmental history of the world's largest downdrift sand system, Fraser Island and Cooloola Coast, Queensland

ACCEPTED MANUSCRIPT

References

Allen, J. R. (1981). Beach erosion as a function of variations in the sediment budget, Sandy Hook, New Jersey, USA. Earth Surface Processes and Landforms, 6(2), 139-150.

Allen, M., and Callaghan, J. (1999). Extreme wave conditions for the south Queensland coastal region. In *Coasts and Ports 1999: Challenges and Directions for the New Century; Proceedings of the 14th Australasian Coastal and Ocean Engineering Conference and the 7th Australasian Port and Harbour Conference* (p. 5). National Committee on Coastal and Ocean Engineering, Institution of Engineers, Australia.

Arinaga, R. A., and Cheung, K. F. (2012). Atlas of global wave energy from 10 years of reanalysis and hindcast data. *Renewable Energy*, *39*(1), 49-64.

Barnard, P. L., Short, A. D., Harley, M. D., Splinter, K. D., Vitousek, S., Turner, I. L., ... and Hansen, J. E. (2015). Coastal vulnerability across the Pacific dominated by El Nino/Southern oscillation. *Nature Geoscience*, *8*(10), 801-807.

Bureau of Meteorology (BoM). (2017). Southern Oscillation Index (SOI) since 1876. Retrieved online 1 June 2017 from: http://www.bom.gov.au/climate/enso/soi/

Berens, P. (2009). CircStat: A Matlab Toolbox for Circular Statistics. *Journal of Statistical Software*, Volume 31, Issue 10, 2009

Blivi, A., Anthony, E. J., and Oyédé, L. M. (2002). Sand barrier development in the bight of Benin, West Africa. Ocean & coastal management, 45(2), 185-200.

Browne, M., Castelle, B., Strauss, D., Tomlinson, R., Blumenstein, M., and Lane, C. (2007). Near-shore swell estimation from a global wind-wave model: Spectral process, linear, and artificial neural network models. *Coastal Engineering*, *54*(5), 445-460.

Browning, S. A., and Goodwin, I. D. (2013). Large-scale influences on the evolution of winter subtropical maritime cyclones affecting Australia's east coast. *Monthly Weather Review*, *141*(7), 2416-2431.

Callaghan, J., and Power, S. B. (2014). Major coastal flooding in southeastern Australia 1860–2012, associated deaths and weather systems. *Australian Meteorological and Oceanographic Journal*, *64*, 183-213.

Camus, P., Cofiño, A. S., Mendez, F. J., and Medina, R. (2011). Multivariate wave climate using self-organizing maps. *Journal of Atmospheric and Oceanic technology*, *28*(11), 1554-1568.

Castelle, B., Marieu, V., Bujan, S., Splinter, K. D., Robinet, A., Sénéchal, N., and Ferreira, S. (2015). Impact of the winter 2013–2014 series of severe Western Europe storms on a double-barred sandy coast: Beach and dune erosion and megacusp embayments. Geomorphology, 238, 135-148.

Chawla, A., Spindler, D., and Tolman, H. (2012). 30 Year Wave Hindcasts using WAVEWATCH IIIR c with CFSR winds Phase I. U.S. Department of Commerce National Oceanic and Atmospheric Administration National Weather Service.

Church, J. A. (1987). East Australian Current adjacent to the Great Barrier Reef. *Marine and Freshwater Research*, *38*(6), 671-683.

Clarke, K. R., and Warwick, R. M. (1994). An approach to statistical analysis and interpretation. *Change in marine communities*, *2*.

Clark, P. U., Pisias, N. G., Stocker, T. F., and Weaver, A. J. (2002). The role of the thermohaline circulation in abrupt climate change. Nature, 415(6874), 863-869.

Coelho, C., Silva, R., Veloso-Gomes, F., and Taveira-Pinto, F. (2009). Potential effects of climate change on northwest Portuguese coastal zones. *ICES Journal of Marine Science*, *66*(7), 1497-1507.

Coles, S., Bawa, J., Trenner, L., and Dorazio, P. (2001). *An introduction to statistical modeling of extreme values* (Vol. 208). London: Springer.

Cooper, J. A. G., Jackson, D. W. T., Navas, F., McKenna, J., and Malvarez, G. (2004). Identifying storm impacts on an embayed, high-energy coastline: examples from western Ireland. *Marine Geology*, *210*(1), 261-280.

Cornett, A. M. (2008). A global wave energy resource assessment. In *The Eighteenth International Offshore and Polar Engineering Conference*. International Society of Offshore and Polar Engineers.

Costas, S., Alejo, I., Rial, F., Lorenzo, H., and Nombela, M. A. (2006). Cyclical evolution of a modern transgressive sand barrier in Northwestern Spain elucidated by GPR and aerial photos. Journal of sedimentary Research, 76(9), 1077-1092.

Cresswell, G. R., Ellyett, C., Legeckis, R., and Pearce, A. F. (1983). Nearshore features of the East Australian Current system. *Marine and Freshwater Research*, *34*(1), 105-114.

Crowell, M., Leatherman, S. P., and Buckley, M. K. (1991). Historical shoreline change: error analysis and mapping accuracy. *Journal of coastal research*, SI (28) 839-852.

Daly, C. J., Winter, C., and Bryan, K. R. (2015). On the morphological development of embayed beaches. *Geomorphology*, *248*, 252-263.

Davidson, M. A., Turner, I. L., Splinter, K. D., and Harley, M. D. (2017). Annual prediction of shoreline erosion and subsequent recovery. *Coastal Engineering*, *130*, 14-25.

Dissanayake, P., Brown, J., Wisse, P., and Karunarathna, H. (2015). Comparison of storm cluster vs isolated event impacts on beach/dune morphodynamics. Estuarine, Coastal and Shelf Science, 164, 301-312.

Flay, S., and Nott, J. (2007). Effect of ENSO on Queensland seasonal landfalling tropical cyclone activity. *International Journal of Climatology*, *27*(10), 1327-1334.

Fletcher, C., Rooney, J., Barbee, M., Lim, S. C., and Richmond, B. (2003). Mapping shoreline change using digital orthophotogrammetry on Maui, Hawaii. *Journal of Coastal Research*, 106-124.

Flick, R. E. (1993). The myth and reality of southern California beaches. Shore and Beach, 61(3), 3-13.

Goodwin, I. D. (2005). A mid□shelf, mean wave direction climatology for southeastern Australia, and its relationship to the El Niño—Southern Oscillation since 1878 AD. *International Journal of Climatology*, *25*(13), 1715-1729.

Goodwin, I. D., Stables, M. A., and Olley, J. M. (2006). Wave climate, sand budget and shoreline alignment evolution of the Iluka–Woody Bay sand barrier, northern New South Wales, Australia, since 3000 yr BP. Marine Geology, 226(1-2), 127-144.

Goodwin, I. D., T. R. Mortlock, and S. Browning (2016). Tropical and extratropical-origin storm wave types and their influence on the East Australian longshore sand transport system under a changing climate. J. Geophys. Res. Oceans, 121, doi:10.1002/2016JC011769.

Gourlay, M. R. 1975. Wave climate and design waves at Moffat beach-A specific analysis with some general implications. In *Second Australian Conference on Coastal and Ocean Engineering, 1975: The Engineer, the Coast and the Ocean* (p. 161). Institution of Engineers, Australia.

Grant, A. P., Walsh, K. J. 2001. Interdecadal variability in north□east Australian tropical cyclone formation. *Atmospheric Science Letters*, *2*(1□4), 9-17.

Gurran, N. (2008). The turning tide: Amenity migration in coastal Australia. *International Planning Studies*, *13*(4), 391-414.

Harley, M. D., Turner, I. L., Short, A. D., and Ranasinghe, R. (2010). Interannual variability and controls of the Sydney wave climate. *International Journal of Climatology*, *30*(9), 1322-1335.

Harley, M. D., Turner, I. L., Short, A. D., and Ranasinghe, R. (2011). A reevaluation of coastal embayment rotation: The dominance of cross□shore versus alongshore sediment transport processes, Collaroy□Narrabeen Beach, southeast Australia. *Journal of Geophysical Research: Earth Surface*, 116(F4).

Harley, M. D., Turner, I. L., Kinsela, M. A., Middleton, J. H., Mumford, P. J., Splinter, K. D., ... and Short, A. D. (2017). Extreme coastal erosion enhanced by anomalous extratropical storm wave direction. *Scientific reports*, 7(1), 6033.

Harris, P. T., Heap, A. D., Bryce, S. M., Porter-Smith, R., Ryan, D. A., and Heggie, D. T. (2002). Classification of Australian clastic coastal depositional environments based upon a quantitative analysis of wave, tidal, and river power. *Journal of Sedimentary Research*, *72*(6), 858-870.

Harvey, N., and Woodroffe, C. D. (2008). Australian approaches to coastal vulnerability assessment. *Sustainability Science*, *3*(1), 67-87.

Hemer, M. A., Church, J. A., and Hunter, J. R. (2007). Waves and climate change on the Australian coast. *Journal of Coastal Research*, *50*, 432-437.

Hemer, M. A., Church, J. A., and Hunter, J. R. (2010). Variability and trends in the directional wave climate of the Southern Hemisphere. *International Journal of Climatology*, *30*(4), 475-491.

Hemer, M. A., McInnes, K. L., and Ranasinghe, R. (2012). Climate and variability bias adjustment of climate model-derived winds for a southeast Australian dynamical wave model. *Ocean Dynamics*, *62*(1), 87-104.

Hemer, M. A., Fan, Y., Mori, N., Semedo, A., and Wang, X. L. (2013). Projected changes in wave climate from a multi-model ensemble. *Nature climate change*, *3*(5), 471.

Hughes, L. (2003). Climate change and Australia: trends, projections and impacts. *Austral Ecology*, *28*(4), 423-443.

Hughes, M. G., and Heap, A. D. (2010). National-scale wave energy resource assessment for Australia. *Renewable Energy*, 35(8), 1783-1791.

Hugo, G. (2008). Immigrant settlement outside of Australia's capital cities. *Population, Space and Place*, *14*(6), 553-571.

IPCC. (2013). Climate Change 2013: The Physical Science Basis. Contribution of Working Group I to the Fifth Assessment Report of the Intergovernmental Panel on Climate Change [Stocker, T.F., D. Qin, G.-K. Plattner, M. Tignor, S.K. Allen, J. Boschung, A. Nauels, Y. Xia, V. Bex and P.M. Midgley (eds.)]. Cambridge University Press, Cambridge, United Kingdom and New York, NY, USA, 1535 pp.

Karunarathna, H., Pender, D., Ranasinghe, R., Short, A. D., Reeve, D. E. 2014. The effects of storm clustering on beach profile variability. *Marine Geology*, *348*, 103-112.

Kasper□Zubillaga, J. J., Ortiz□Zamora, G., Dickinson, W. W., Urrutia□Fucugauchi, J., & Soler□Arechalde, A. M. (2007). Textural and compositional controls on modern beach and dune sands, New Zealand. Earth Surface Processes and Landforms, 32(3), 366-389.

Lehmann, J., and Coumou, D. (2015). The influence of mid-latitude storm tracks on hot, cold, dry and wet extremes. Scientific reports, 5, 17491.

Lewis, S. E., Sloss, C. R., Murray-Wallace, C. V., Woodroffe, C. D., and Smithers, S. G. (2013). Post-glacial sea-level changes around the Australian margin: a review. *Quaternary Science Reviews*, *74*, 115-138.

Liu, Y., and R. H. Weisberg (2011). A review of self-organizing map applications in meteorology and oceanography. Self-Organizing Maps: Applications and Novel Algorithm Design, J. I. Mwasiagi, Ed., *InTech*, 253–272, doi:10.5772/13146

Loureiro, C., Ferreira, O., and Cooper, J. A. G. (2009). Contrasting morphologic behaviour at embayed beaches in Southern Portugal. Journal of coastal research, 83-87.

Masselink, G., Scott, T., Poate, T., Russell, P., Davidson, M., and Conley, D. (2016). The extreme 2013/2014 winter storms: hydrodynamic forcing and coastal response along the southwest coast of England. Earth Surface Processes and Landforms, 41(3), 378-391.

Martin, L., and Suguio, K. (1992). Variation of coastal dynamics during the last 7000 years recorded in beach-ridge plains associated with river mouths: example from the central Brazilian coast. Palaeogeography, Palaeoclimatology, Palaeoecology, 99(1-2), 119-140.

Mazas, F., and Hamm, L. (2011). A multi-distribution approach to POT methods for determining extreme wave heights. *Coastal Engineering*, *58*(5), 385-394.

Moore, L. J., Ruggiero, P., and and List, J. H. (2006). Comparing mean high water and high water line shorelines: should proxy-datum offsets be incorporated into shoreline change analysis?. *Journal of Coastal Research*, 894-905.

Mortlock, T. R., and Goodwin, I. D. (2015). Directional wave climate and power variability along the Southeast Australian shelf. *Continental Shelf Research*, *98*, 36-53.

Nichol, S. L., McPherson, A., Davies, G., Jiang, W., Howard, F., Gravois, U., ... and Baldock, T. (2016). A Framework for Modelling Shoreline Response to Clustered Storm Events: A Case Study from Southeast Australia. *Journal of Coastal Research*, 75(sp1), 1197-1201.

Nott, J., Chague□Goff, C., Goff, J., Sloss, C., and Riggs, N. (2013). Anatomy of sand beach ridges: evidence from severe Tropical Cyclone Yasi and its predecessors, northeast Queensland, Australia. *Journal of Geophysical Research: Earth Surface*, *118*(3), 1710-1719.

Ojeda, E., and Guillén, J. (2008). Shoreline dynamics and beach rotation of artificial embayed beaches. Marine Geology, 253(1), 51-62.

Pajak, M. J., and Leatherman, S. (2002). The high water line as shoreline indicator. *Journal of Coastal Research*, Vol. 18, No. 2 329-337.

Peel, M. C., Finlayson, B. L., and McMahon, T. A. (2007). Updated world map of the Köppen-Geiger climate classification. *Hydrology and earth system sciences discussions*, *4*(2), 439-473.

Pender, D., Callaghan, D. P., and Karunarathna, H. (2015). An evaluation of methods available for quantifying extreme beach erosion. *Journal of Ocean Engineering and Marine Energy*, *1*(1), 31-43.

Phinn, S. R., and Hastings, P. A. (1992). Southern Oscillation influences on the wave climate of south-eastern Australia. *Journal of Coastal Research*, 579-592.

Pinto, C. A., Taborda, R., Andrade, C., and Teixeira, S. B. (2009). Seasonal and mesoscale variations at an embayed beach (Armação de Pera, Portugal). Journal of Coastal Research, 118-122.

Power S, Casey T, Folland C, Colman A, and Mehta V. 1999. Interdecadal modulation of the impact of ENSO on Australia. Climate Dynamics 15: 319–324

Power, S., Haylock, M., Colman, R., Wang, X. 2006. The predictability of interdecadal changes in ENSO activity and ENSO teleconnections. *Journal of Climate*, *19*(19), 4755-4771.

Queensland Government. (2017) (a). *Queensland Tidal Planes.* Retrieved 1 June 2017 from: https://www.msq.qld.gov.au/Tides/Tidal-planes

Queensland Government. (2017) (b). Queensland Spatial Catalogue - QSpatial aerial imagery. Retrieved 1 June 2017 from: http://qldspatial.information.qld.gov.au/catalogue/custom/index.page

Roy, P. S., and Crawford, E. A. (1977). Significance of sediment distribution in major coastal rivers, northern NSW. In *Third Australian Conference on Coastal and Ocean Engineering, 1977: The Coast, the Ocean and Man, The*(p. 173). Institution of Engineers, Australia.

Roy, P. S., and Thom, B. G. (1981). Late Quaternary marine deposition in New South Wales and southern Queensland—an evolutionary model. *Journal of the Geological Society of Australia*, *28*(3-4), 471-489.

Ranasinghe, R., McLoughlin, R., Short, A., and Symonds, G. (2004). The Southern Oscillation Index, wave climate, and beach rotation. *Marine Geology*, *204*(3), 273-287.

Rousseeuw, P. J. (1987). Silhouettes: a graphical aid to the interpretation and validation of cluster analysis. *Journal of computational and applied mathematics*, *20*, 53-65.

Salinger, M. J., Renwick, J. A., Mullan, A. B. 2001. Interdecadal Pacific oscillation and south Pacific climate. *International Journal of Climatology*, *21*(14), 1705-1721.

Sanford, L. P., and Gao, J. (2017). Influences of wave climate and sea level on shoreline erosion rates in the Maryland Chesapeake Bay. *Estuaries and Coasts*, 1-19.

Seidel, D. J., Fu, Q., Randel, W. J., Reichler, T. J. 2008. Widening of the tropical belt in a changing climate. *Nature geoscience*, *1*(1), 21-24.

Shand, T. D., Cox, R. J., Mole, M. A., Carley, J. T., and Peirson, W. L. (2011). Coastal storm data analysis: provision of extreme wave data for adaptation planning. In *Coasts and Ports 2011: Proceedings of the 20th Australasian Coastal and Ocean Engineering Conference and the 13th Australasian Port and Harbour Conference* (p. 170). Engineers Australia.

Short, A. D., and Trembanis, A. C. (2004). Decadal scale patterns in beach oscillation and rotation Narrabeen Beach, Australia—time series, PCA and wavelet analysis. *Journal of Coastal Research*, 523-532.

Short, A. D., Trembanis, A. C., and Turner, I. L. (2001). Beach oscillation, rotation and the Southern oscillation, Narrabeen Beach, Australia. In *Coastal Engineering 2000* (pp. 2439-2452).

Siegle, E., and Asp, N. E. (2007). Wave refraction and longshore transport patterns along the southern Santa Catarina coast. Brazilian Journal of Oceanography, 55(2), 109-120.

Sloss, C. R., Murray-Wallace, C. V., and Jones, B. G. (2007). Holocene sea-level change on the southeast coast of Australia: a review. *The Holocene*, *17*(7), 999-1014.

Smith, A. M., Mather, A. A., Bundy, S. C., Cooper, J. A. G., Guastella, L. A., Ramsay, P. J., and Theron, A. (2010). Contrasting styles of swell-driven coastal erosion: examples from KwaZulu-Natal, South Africa. Geological Magazine, 147(6), 940-953.

Sofian, I., and Wijanarto, A. B. (2010). Simulation of Significant Wave Height Climatology using WaveWatch III. *International Journal of Geoinformatics*, 6(4).

Sohn, S. J., Tam, C. Y., Jeong, H. I. 2016. How do the strength and type of ENSO affect SST predictability in coupled models. *Scientific reports*, *6*, 33790.

Speer, M. S., Wiles, P., and Pepler, A. (2009). Low pressure systems off the New South Wales coast and associated hazardous weather: establishment of a database. *Australian Meteorological and Oceanographic Journal*, *58*(1), 29.

Splinter, K. D., Davidson, M. A., Golshani, A., and Tomlinson, R. (2012). Climate controls on longshore sediment transport. *Continental Shelf Research*, *48*, 146-156.

Splinter, K. D., Turner, I. L., Davidson, M. A., Barnard, P., Castelle, B., and Oltman□Shay, J. (2014). A generalized equilibrium model for predicting daily to interannual shoreline response. *Journal of Geophysical Research: Earth Surface*, *119*(9), 1936-1958.

Strauss, D., Mirferendesk, H., and Tomlinson, R. (2007). Comparison of two wave models for Gold Coast, Australia. In *Proceedings of the 9th International Coastal Symposium. Journal of Coastal Research, Special Issue*(No. 50, pp. 312-316).

Stone, G. W., Stapor, F. W., May, J. P., and Morgan, J. P. (1992). Multiple sediment sources and a cellular, non-integrated, longshore drift system: Northwest Florida and southeast Alabama coast, USA. Marine Geology, 105(1-4), 141-154.

Thieler, E. R., Himmelstoss, E. A., Zichichi, J. L., and Ergul, A. (2009). *The Digital Shoreline Analysis System (DSAS) version 4.0-an ArcGIS extension for calculating shoreline change* (No. 2008-1278). US Geological Survey.

Thomas, T., Phillips, M. R., and Williams, A. T. (2010). Mesoscale evolution of a headland bay: Beach rotation processes. *Geomorphology*, *123*(1-2), 129-141.

Thomas, T., Phillips, M. R., Williams, A. T., and Jenkins, R. E. (2011). Short-term beach rotation, wave climate and the North Atlantic Oscillation (NAO). *Progress in Physical Geography*, 35(3), 333-352.

Tibshirani, R., Walther, G., and Hastie, T. (2001). Estimating the number of clusters in a data set via the gap statistic. *Journal of the Royal Statistical Society: Series B (Statistical Methodology)*, *63*(2), 411-423.

Tolman, H. L. (2009). User manual and system documentation of WAVEWATCH III TM version 3.14. *Technical note, MMAB Contribution*, *276*, 220.

Trenberth, K. E., and Hurrell, J. W. (1994). Decadal atmosphere-ocean variations in the Pacific. Climate Dynamics, 9(6), 303-319.

Tribe, H. M., and Kennedy, D. M. (2010). The geomorphology and evolution of a large barrier spit: Farewell Spit, New Zealand. Earth Surface Processes and Landforms, 35(15), 1751-1762.

US Army Corp. Of Engineers. (USACE). 1984. *Shore Protection Manual 4th edition*. Department of the Army Waterways Experiment Station. US Government Printing Office, Washington, DC.

Vousdoukas, M. I., Almeida, L. P. M., Ferreira, Ó. 2012. Beach erosion and recovery during consecutive storms at a steep□sloping, meso□tidal beach. *Earth Surface Processes and Landforms*, *37*(6), 583-593.

Walsh, K. J. E., Nguyen, K. C., McGregor, J. L. 2004. Fine-resolution regional climate model simulations of the impact of climate change on tropical cyclones near Australia. *Climate Dynamics*, *22*(1), 47-56.

You, Z. J. (2011). Extrapolation of historical coastal storm wave data with best-fit distribution function. *Australian Journal of Civil Engineering*, *9*(1), 73-82.

You, Z. J., and Lord, D. (2008). Influence of the El Niño–Southern Oscillation on NSW Coastal Storm Severity. *Journal of Coastal Research*, *24*(sp2), 203-207.

Figure captions:

Figure 1. Study area showing the section of coast used for shoreline change analysis. The grid point used for wave hindcast reanalysis (NOAA WAVEWATCH III) (-25.9°S, 153.73°E) is indicated on the map of Australia.

[1.5 column figure size]

Figure 2. Mean monthly wave data for the study region (1979-2009) showing variability in: (a) wave direction (Dp); (b) significant wave height (Hs); and (c) primary peak spectral wave period (Tp).

[1 column figure size]

Figure 3a-b. Directional distribution of storm events showing (a) a bimodal distribution of directionality, and (b) wave directional rose for the storm events. P1 refers to peak 1 and P2 refers to peak 2 of the directional distribution of storm wave events. The peaks represent the most frequent waves within each distribution of a certain direction range.

[1.5 column figure size]

Figure 4. K-Means cluster analysis of two storm wave climates using the normalised parameters: significant wave height (Hs), wave direction (Dp), and primary peak spectral wave period (Tp). Type 1 and 2 corresponds with the two cluster groups output by K-means and GMM.

[1 column figure size]

Figure 5a-b. GMM cluster analysis of two storm wave climates: (a) wave direction and significant wave height; (b) direction and wave period. Data is normalised as per Camus et al. (2011) to maintain similar weightings of parameters.

[1.5 column figure size]

Figure 6a-b. Distribution (PDF) of (a) Hs and (b) Dp for La Nina (SOI ≥ +7) (37 months total) and El Nino (SOI ≤ -7) (64 months total) periods sustained ≥ 6 months in duration. Cumulative distribution function included for both. Mean SOI for El Nino periods: SOI -16.87 (median -16.65) and mean SOI for La Nina periods: SOI 12.74 (median 12.20).

[2 column figure size]

Figure 7. (a) Rate of shoreline change for the whole beach 1958-2012; (b) net shoreline movement over time; (c) rate of shoreline change for the whole study area.

[2 column figure size]

Figure 8. (a) Mean monthly sea surface temperature (SST) anomaly and net shoreline movement. SST anomaly > +1°C shown in grey boxes with max anomaly annotated; (b) Mean monthly SOI and net shoreline movement. Dashed lines show classified La Nina and El Nino threshold; (c) mean monthly Hs and net shoreline movement. Hindcast wave record starts at 1979 with the 2010-2012 wave data added from NOAA's global 30m model; (d) Mean monthly wave direction and net shoreline movement; cross correlations between (e) mean monthly SOI and mean monthly SST anomaly (1958-2012) with maximum correlations at -4 and +9 month lags; (f) mean monthly SST and Hs anomalies (1979-2012) with maximum correlations at -8 and +6 month lags.

[1.5 column figure size]

Tables and table captions:

Table 1. Descriptive statistics of the modal offshore wave climate for the study region (1979-2009) including mean daily significant wave height (Hs), wave direction (Dp), and primary peak spectral wave period (Tp). Data hindcast from the NOAA WAVEWATCH III wave model.

Descriptive statistics	Hs (m)	Dp (°N)	Tp (sec)
Mean	1.91	128.96	8.60
Median	1.76	117.22	8.53
Mode	2.08	92.22	8.49
St Dev.	0.77	49.12	1.74
90th percentile	2.93	166.03	10.85
10th percentile	1.09	87.85	6.41

Table 2. Storm wave climate cluster centres identified from K-means cluster analysis, CircStat, and Gaussian Mixture Models showing similar cluster centres. Wave parameters include significant wave height (Hs), wave direction (Dp), primary peak spectral wave period (Tp), and storm duration. For seasonality of storm occurrence, summer = 1, autumn = 2, winter = 3 and spring = 4.

K-Means final cluster centres (mu)		
	Cluster 1	**Cluster 2**
Season	1.98	2.31
Hs (m)	3.73	3.54
Dp (°N)	106.20	142.20
Tp (sec)	9.51	9.38
Duration (days)	4.71	3.79
n	105	52
Circ Stat final cluster centres		
	Cluster 1	**Cluster 2**
Mean resultant vector (°N)	106.07	142.99
Median Dp (°N)	106.57	143.20
Standard deviation (°)	10.25	10.63
n	105	52
GMM final cluster centres (mu)		
Model 1: Hs vs Dp	**Cluster 1**	**Cluster 2**
Dir (°N)	106.20	143.50
Hs (m)	3.73	3.54
Model 2: Tp vs Dp	**Cluster 1**	**Cluster 2**
Dir (°N)	106.90	143.80
Tp (sec)	9.53	9.37
n	105	52

Table 3. a. Pearson correlation analysis between mean annual SOI and wave data 1979-2009. SOI is the mean annual SOI index value (BoM, 2017), Hs is mean annual significant wave height, Dp is mean annual wave direction, Tp is mean annual wave period, SF is annual storm frequency, SD is mean annual storm duration, D >Hs_{10} refers to total annual days over Hs_{10} threshold (2.93 m), and SST a is the mean annual SST anomaly. b. Correlations between net shoreline movement (NSM) and 6-month pre-image SST anomaly (SST a), Hs, Hs anomaly (Hs a), Dp, Tp, and SOI 1979-2012.

a. Correlations between mean annual SOI, SST anomaly, and annual scale wave/storm data

		SOI	Hs	Dp	Tp	SF	SD	D >Hs_{10}	SST a
SOI	Pearson correlation	1	0.505**	-0.362*	0.415*	0.367*	-0.357*	0.422*	0.196
	Sig. (2-tailed)		0.004	0.045	0.02	0.042	0.49	0.018	0.290
Hs	Pearson correlation	0.505**	1	-0.495**	0.628**	0.719**	-0.111	0.862**	0.414*
	Sig. (2-tailed)	0.004		0.005	0	0	0.554	0	0.021
Dp	Pearson correlation	-0.362*	-0.495**	1	-0.464**	-0.245	0.261	-0.253	-0.176
	Sig. (2-tailed)	0.045	0.005		0.009	0.185	0.156	0.169	0.344
Tp	Pearson correlation	0.415*	0.628**	-0.464**	1	0.241	-0.206	0.345	0.186
	Sig. (2-tailed)	0.02	0	0.009		0.191	0.267	0.058	0.316
Storm F.	Pearson correlation	0.367*	0.719**	-0.245	0.241	1	-0.255	0.855**	0.450*
	Sig. (2-tailed)	0.042	0	0.185	0.191		0.165	0	0.011
Storm D.	Pearson correlation	-0.357*	-0.111	0.261	-0.206	-0.255	1	0.280	-0.106
	Sig. (2-tailed)	0.042	0.554	0.156	0.267	0.165		0	0.571
D >Hs_{10}	Pearson correlation	0.422*	0.862**	-0.253	0.345	0.855**	0.280	1	0.322
	Sig. (2-tailed)	0.018	0	0.169	0.058	0	0.883		0.078
SST A.	Pearson correlation	.196	.414*	-.176	.186	.450*	-.106	.322	1
	Sig. (2-tailed)	.290	.021	.344	.316	.011	.571	.078	

b. Correlations between net shoreline movement and 6-month pre-image SST anomaly, SOI, and wave data

		NSM	Hs	Hs a	Dir	Tp	SST a	SOI
NSM	Pearson correlation	1	-0.418	-0.646*	0.552*	-0.294	-0.592*	-0.459
	Sig. (2-tailed)		0.137	0.013	0.041	0.308	0.026	0.099
Hs	Pearson correlation	-0.418	1	0.652*	-0.892**	0.624*	0.279	0.381
	Sig. (2-tailed)	0.137		0.011	0.000	0.017	0.335	0.171
Hs A.	Pearson correlation	-0.646*	0.652*	1	-0.529	0.393	0.616*	0.681**
	Sig. (2-tailed)	0.013	0.011		0.052	0.165	0.019	0.022
Dp	Pearson correlation	0.552*	-0.892**	-0.529	1	-.445	-0.369	-0.396
	Sig. (2-tailed)	.041	0.000	0.052		.111	0.194	0.161
Tp	Pearson correlation	-.294	0.624*	0.393	-0.445	1	-0.162	-0.035
	Sig. (2-tailed)	.308	0.017	0.165	0.111		0.581	0.906
SST A.	Pearson correlation	-0.592*	0.279	.616*	-.369	-.162	1	0.789**
	Sig. (2-tailed)	0.026	0.335	.019	.194	.581		0.001
SOI	Pearson correlation	-0.4596	0.381	0.681**	-0.396	-0.035	0.789**	1
	Sig. (2-tailed)	0.099	0.171	0.022	0.161	0.906	0.001	

** Correlation is significant at the 0.01 level (2-tailed).

* Correlation is significant at the 0.05 level (2-tailed).

Highlights

- Storms in SEQ are delineated into two types: ex-tropical storms and East Coast Lows.
- The Southern Oscillation Index is positively correlated to Hs and storm frequency
- Periods of sustained La Nina increase Hs by 0.10 m and shift mean wave direction 6° anticlockwise.
- Shoreline erosion and deposition is closely tied to variability in wave height and direction, modulated by underlying ENSO signals.
- Clusters of storms in rapid succession is a major driver of coastal erosion.

Regional index terms

Australia, Queensland, Inskip Peninsula